

1 **Title**

2
3 Synthetic mycobacterial molecular patterns work synergistically to recapitulate complete
4 Freund's adjuvant

5
6 **Authors/Affiliations**

7
8 Jean-Yves Dubé^{1,2,3*}, Fiona McIntosh^{2,3}, Juan G. Zarruk⁴, Samuel David⁴, Jérôme Nigou⁵,
9 Marcel A. Behr^{1,2,3,6*}

10
11 1, Department of Microbiology and Immunology, McGill University. 2, Infectious diseases and
12 Immunity in Global Health Program, Research Institute of the McGill University Health Centre.
13 3, McGill International TB Centre. 4, Centre for Research in Neuroscience, Research Institute of
14 the McGill University Health Centre. 5, Institut de Pharmacologie et de Biologie Structurale,
15 Université de Toulouse, CNRS, Université Paul Sabatier, Toulouse, France. 6, Department of
16 Medicine, McGill University Health Centre, Montréal, Canada.

17
18 **Contact Info***

19
20 jean-yves.dube@mail.mcgill.ca
21 marcel.behr@mcgill.ca
22 McGill University Health Centre
23 1001 boul. Décarie
24 Glen Site Block E, Office #EM3.3212
25 Montréal, Québec, Canada
26 H4A 3J1

27
28 **Abstract**

29
30 Complete Freund's adjuvant (CFA) has historically been one of the most useful tools of
31 immunologists. Essentially comprised of dead mycobacteria and mineral oil, we asked ourselves
32 what is special about the mycobacterial part of this adjuvant, and could it be recapitulated
33 synthetically? Here, we demonstrate the essentiality of *N*-glycolylated peptidoglycan plus
34 trehalose dimycolate (both unique in mycobacteria) for the complete adjuvant effect using
35 knockouts and chemical complementation. A combination of synthetic *N*-glycolyl muramyl
36 dipeptide and minimal trehalose dimycolate motif GlcC14C18 was able to induce experimental
37 autoimmunity qualitatively similar to the whole mycobacteria in CFA. This research outlines
38 how to replace CFA with a consistent, molecularly defined adjuvant which may inform the
39 design of immunotherapeutic agents and vaccines benefitting from cell-mediated immunity. We
40 also anticipate using synthetic microbe-associated molecular patterns (MAMPs) to study
41 mycobacterial immunity and immunopathogenesis.

42
43
44
45
46

47 Introduction

48
49 Infection with *Mycobacterium tuberculosis*, or administration of bacille Calmette-Guérin
50 (BCG), normally leads to cell-mediated immunity (CMI) to the corresponding bacterial
51 antigens. The tuberculin skin test is positive when the immune response, a type IV
52 hypersensitivity reaction or delayed-type hypersensitivity (DTH), occurs to tuberculin (a protein
53 extract of *M. tuberculosis*). This “cutaneous sensitivity” was closely examined in the 1940s
54 using complete Freund’s adjuvant (CFA, heat-killed *M. tuberculosis* in mineral oil plus
55 surfactant)^{1,2}. These studies provided the first direct evidence for the cellular nature of DTH by
56 transfer from a CFA-immunized guinea pig to a naïve one only through the washed, heat-labile
57 cellular fraction of peritoneal exudates^{1,2}. It is now known that DTH is mediated specifically by
58 antigen-sensitive T cells.

59
60 Today, CFA is a ‘gold standard’ adjuvant for eliciting CMI in research models of
61 autoimmune disease. Notable is the experimental autoimmune encephalomyelitis (EAE) model
62 of T-cell mediated destruction of myelin causing ascending paralysis, used most often to model
63 multiple sclerosis^{3,4}. CFA is not used in humans because of high reactogenicity⁵. We have
64 asked ourselves: what was the impetus for Jules Freund to develop his eponymous adjuvant with
65 *M. tuberculosis*? For those conducting TB research, it is well appreciated that handling *M.*
66 *tuberculosis* (a slow growing, clumping, fastidious, and lethally pathogenic organism) is a
67 significant task *per se*. So, why did Freund choose to incorporate these bacteria?

68
69 Effort has been made to describe the microbe-associated molecular patterns (MAMPs) in
70 mycobacteria that drive the adjuvant effect. Evidence has pointed to mycobacterial
71 peptidoglycan (PGN), specifically down to the molecular motif muramyl dipeptide (MDP)^{6,7}.
72 Mycobacteria are distinct in that they produce the *N*-glycolyl MDP motif in their cell wall^{8,9,10}
73 and this PGN modification has been shown to be more potent compared to the common *N*-acetyl
74 MDP motif possessed by other bacteria^{7,11}. MDP is thought to be recognized through the host
75 molecule NOD2¹², and mutations in NOD2 predispose humans to increased risk of
76 mycobacterial and inflammatory diseases^{13,14,15,16}. Alternatively, others have pointed to the
77 mycobacterial cell wall lipid trehalose-6,6-dimycolate (TDM) alone or synergistically with
78 purified peptidoglycan¹⁷. TDM is recognized by the host with the C-type lectin Mincle in
79 concert with FcR γ and MCL^{18,19}. TDM has been demonstrated in animal models to alone be
80 sufficient for granuloma formation and immunopathological responses^{18,20}.

81
82 Both *N*-glycolyl MDP and TDM are MAMPs unique to mycobacteria. Their role in
83 mycobacterial immune responses is supported by the literature and their host receptors are well-
84 known. Additionally, *N*-glycolyl MDP is producible synthetically^{7,21,22}. Recently a minimal
85 motif of TDM called GlcC14C18 was produced synthetically and shown to retain adjuvancy but
86 with minimal toxicity²³. As a complex biologic, CFA is subjected to batch inconsistency. We
87 hypothesized that it is possible to create an entirely synthetic CFA using a rational approach to
88 identify essential MAMPs to replace the whole mycobacteria in the adjuvant. In this work, we
89 establish the necessity for *N*-glycolylation of PGN, NOD2 and Mincle for full CFA adjuvancy.
90 We also demonstrate that the mycobacteria in CFA can be replaced with synthetic *N*-glycolyl
91 MDP and GlcC14C18 to at least partially restore the adjuvant effect in both a murine model of
92 antigen-specific T-cell immunity as well as the EAE model of autoimmune ascending paralysis.

93 MAMPs worked synergistically, highlighting the need for considering more than one MAMP in
94 adjuvant design. An entirely synthetic adjuvant may benefit animal experiments currently using
95 CFA as well as indicate how to translate the CFA effect into products for human use. We
96 suggest such synthetics may be used to dissect immuno-pathogenesis of mycobacterial diseases.

97

98 **Results**

99

100 *N*-glycolylation of PGN is required for complete mycobacterial adjuvancy

101

102 Previous work from our group indicated mycobacteria required *N*-glycolylated PGN to
103 elicit a maximal immune response during live infection^{7,11}. To determine if CMI elicited from
104 dead mycobacteria in the context of Freund's adjuvant similarly required *N*-glycolylated PGN,
105 we prepared in-house complete Freund's adjuvant with heat-killed *M. tuberculosis* strain H37Rv,
106 and H37Rv $\Delta namH$. NamH is the enzyme responsible for *N*-glycolylation of PGN units as they
107 are being synthesized in the cytoplasm, and the $\Delta namH$ mutant has been characterized
108 previously to be devoid of *N*-glycolylation¹¹ (fig. 1A). We immunized mice against ovalbumin
109 (OVA, an exemplary antigen) with our CFAs, and also with incomplete Freund's adjuvant (IFA,
110 lacks mycobacteria), and examined the OVA-specific T-cell response in the draining lymph
111 nodes seven days later through hallmark cytokine production (fig. 1B; gating in fig. S1). We
112 focused on CD4+CD8- cells because they could significantly produce different cytokines (IL-4,
113 IL-10 and IL-17A in addition to IFN- γ). CD4+CD8- cells were generally the majority OVA-
114 specific IFN- γ producing lymph node cell population and showed greater difference between
115 CFA and IFA immunized mice in terms of OVA-specific IFN- γ (not shown). CD4+CD8- cell
116 responses also correlated very well with IFN- γ ELISpot when tested (not shown). Maximum
117 OVA-specific IFN- γ production from CD4+ T cells was depended on mycobacteria and *namH*;
118 OVA-specific IL-17A was strongly dependent on mycobacteria, but did not depend on *namH*
119 (fig. 1C). We show both percentages and numbers of cells because incorporation of
120 mycobacteria into IFA induced increased lymphocyte numbers in the draining lymph nodes (fig.
121 S2). The data show that *namH* contributes to about one third of mycobacterial-dependent
122 antigen-specific IFN- γ in CD4+ cells (fig. S3). OVA-specific IL-4 and IL-10 were weakly
123 dependent on mycobacteria, but not clearly on *namH* (fig. S2). This is consistent with the
124 hypothesized role for mycobacteria being a key ingredient in CFA for eliciting CMI, and that
125 mycobacterial PGN modification by NamH makes a more potent adjuvant.

126

127 Host *Nod2* is required for complete mycobacterial adjuvancy

128

129 Recognition of mycobacteria during live infection requires the host molecule NOD2²⁴.
130 Because we hypothesize mycobacterial PGN plays a role in CFA adjuvancy, specifically the
131 MDP motif where *N*-glycolylation occurs, we addressed whether the PGN/MDP sensor NOD2 is
132 important for CFA adjuvancy in our OVA model. *Nod2*^{+/+} and *Nod2*^{-/-} mice were immunized
133 against OVA in the context of CFA or IFA of commercial provenance. OVA-specific IFN- γ
134 from CD4+ cells of CFA-immunized mice required *Nod2* for maximal effect (fig. 2), and an
135 independently produced IFN- γ ELISpot of total lymph node cells indicated that *Nod2* is required
136 for about half of the adjuvancy contribution of mycobacteria in CFA (fig. S4A). In the absence
137 of *Nod2*, OVA-specific IL-17A was also impaired in CFA-immunized mice (fig. 2). With IFA
138 as adjuvant, IFN- γ and IL-17A responses were *Nod2*-independent as expected (fig. 2 and S4A).

139 No obvious phenotype was observed for IL-4 and IL-10 (fig. S4C). Together, these results
140 corroborate the role for NOD2 and accordingly mycobacterial PGN in the ability of CFA to elicit
141 CMI.

142 143 Host *Mincle* is required for complete mycobacterial adjuvancy

144
145 In the absence of *Nod2*, the adjuvant effect of mycobacteria declined partially, but not
146 completely. Therefore, there is other mycobacterial MAMP recognition besides that through
147 NOD2 which is important for the remainder CFA adjuvancy. Others have indicated that *Mincle*-
148 mediated recognition of TDM contributes to mycobacterial adjuvancy¹⁷. We tested the
149 dependence of our OVA-immunization model with *Mincle*-KO mice²⁵. *Mincle*^{+/+} and *Mincle*^{-/-}
150 mice were immunized against OVA in the presence of CFA and IFA. CFA-elicited OVA-
151 specific IFN- γ and IL-17A from CD4⁺ T cells was partially dependent on *Mincle* (fig. 3).
152 Similar trends of smaller differences were also observed for IL-4 and IL-10 (fig. S5B). IFA-
153 immunized mice showed *Mincle*-independent responses, as expected (fig. 3 and S5). These
154 results implicate *Mincle* and thus its main mycobacterial ligand, TDM, in CFA adjuvancy as
155 well. Therefore, at least two mycobacterial MAMPs, *N*-glycolylated PGN as well as TDM, are
156 essential for the full adjuvant effect of mycobacteria in the context of CFA.

157 158 Synthetic mycobacterial NOD2 and *Mincle* ligands can complement IFA to increase antigen- 159 specific T-cell responses.

160
161 We have demonstrated that NOD2 and *Mincle* signalling are essential for the full
162 adjuvant effect of CFA. From this line of thought, we hypothesized that IFA can be
163 complemented with pure NOD2 and/or *Mincle* ligands to recapitulate some or all of the adjuvant
164 effect of whole mycobacteria. We initially attempted to complement IFA with *N*-glycolyl MDP
165 alone and TDM alone in our OVA model; neither of these MAMPs produced substantial OVA-
166 specific responses over the IFA baseline in the draining lymph nodes on their own (not shown).
167 TDM administration was limited by pathological inflammation at the injection site with
168 increasing doses, occurring at 10 μ g and higher, which is not observed with CFA injection (fig.
169 S6). Recently, a rationally determined minimal chemical structure of TDM for *Mincle*
170 recognition was produced (called GlcC14C18) (fig. 4A and B) which was reported to retain
171 activity as a *Mincle* agonist without the ‘toxicity’ associated with TDM²³. We compared TDM
172 and GlcC14C18 at a 10 μ g dose in *Mincle*^{+/+} and *Mincle*^{-/-} mice to confirm if GlcC14C18
173 produced less pathological inflammation and whether inflammation was *Mincle*-dependent in our
174 mouse model. Pathological inflammation at the injection site was only observed with TDM, was
175 *Mincle*-dependent (fig. 4C), and worsened over the course of the experiment (fig. S7).

176
177 By examining cytokine production from dendritic cells *in vitro*, it became apparent to us
178 that MDP and TDM elicit maximal immune responses when combined synergistically (fig. S8).
179 Interestingly, GlcC14C18 also synergized with *N*-glycolyl MDP *in vitro* (fig. S8). Using
180 minimal synthetic MAMPs for PGN (i.e. *N*-glycolyl MDP) and TDM (i.e. GlcC14C18), we
181 complemented IFA to test if CMI could be achieved with a completely synthetic adjuvant
182 containing these essential mycobacterial MAMPs. OVA-specific cytokine responses in CD4⁺
183 cells were higher with increasing doses of GlcC14C18 over a 30 μ g *N*-glycolyl MDP dose,
184 relative to MDP alone by flow cytometry (fig. 5); IFN- γ and IL-17A reached only near half of

185 the CFA level at the tested doses, but IL-4 and IL-10 were complemented sufficiently at 10 μ g
186 GlcC14C18. GlcC14C18 clearly induced lymphoproliferation in the draining lymph nodes (fig.
187 S9A), and IFN- γ ELISpot corroborated results obtained with flow cytometry IFN- γ (fig. S9B).
188 To be sure GlcC14C18 adjuvancy was enhanced by addition of MDP *in vivo*, we performed a
189 titration of lower MDP doses on 10 μ g GlcC14C18 which confirmed synergy between the
190 synthetic mycobacterial MAMPs (fig. S10). These results show that mycobacterial adjuvancy in
191 the context of CFA can be at least partially phenocopied synthetically with just two
192 mycobacterial MAMPs: namely *N*-glycolyl MDP and GlcC14C18.

193

194 Synthetic mycobacterial MAMPs can induce EAE similar to CFA

195

196 We were able to partially complement IFA with synthetic mycobacterial MAMPs in our
197 model of OVA immunization according to immunological readouts. One of the common uses of
198 CFA is in animal models of autoantigen-specific autoimmunity. To determine if our synthetic
199 formulation can phenocopy the effect of whole mycobacteria to produce a more complex
200 biological outcome such as autoimmunity, and thereby provide further validation of the
201 ‘completeness’ of the synthetic formula, we tested IFA + GlcC14C18 + *N*-glycolyl MDP against
202 CFA in ability to induce relapsing-remitting EAE (RR-EAE). Briefly, mice were randomly
203 immunized against myelin oligodendrocyte glycoprotein (MOG) synthetic peptide with CFA or
204 IFA + 10 μ g GlcC14C18 + 30 μ g *N*-glycolyl MDP, and onset of RR-EAE was determined by
205 clinically scoring ascending paralysis daily in a blinded manner (fig. 6A). Both CFA and IFA +
206 GlcC14C18 + MDP produced RR-EAE that was indistinguishable except quantitatively: over the
207 course of the experiment, the average EAE score was lower with the synthetic adjuvant
208 compared to the CFA control (fig. 6B), with a cumulative score suggesting about half the disease
209 burden (58% of CFA cumulative score) (fig. 6C). Expectedly, lower EAE scores also
210 corresponded with less weight-loss (fig. S11A). Of note, there were mice in the synthetic
211 adjuvant group that reached the same scores as in the CFA group, but fewer (fig. S11B).
212 Therefore, GlcC14C18 and *N*-glycolyl MDP were sufficient to recapitulate the adjuvant effect of
213 the whole mycobacterial cell in EAE, albeit quantitatively less at the tested doses of MAMPs.
214 Additionally, we had attempted RR-EAE with IFA + TDM + MDP previously, which produced a
215 far less compelling phenocopy of CFA (fig. S12). In our hands, the IFA + GlcC14C18 + *N*-
216 glycolyl MDP adjuvant has both the advantage of being completely synthetic and more
217 efficacious, than the TDM-containing adjuvant.

218

219 To verify if there were any overt qualitative histopathological differences in EAE
220 between CFA and the synthetic adjuvant, we examined spinal cords from three mice from each
221 adjuvant group, having EAE scores 2, 3 and 3.5 at harvest (disease profile of these mice in fig.
222 S11C). Both cellular infiltrates and demyelination of the white matter looked equivalent
223 between adjuvants upon visual inspection (fig. 7A). Mice with different EAE scores had
224 correspondingly different areas of diseased tissue of the spinal cord (fig. 7B), but in comparing
225 adjuvants there was no detectable difference in the area of diseased spinal cord tissue (with
226 statistical power to detect as low as +/- 15% CFA levels) (fig. 7C). The main determining
227 variable was EAE score, not adjuvant. Overall, we were not able to detect any overt differences
228 in the autoimmune pathology created by IFA + GlcC14C18 + MDP compared to the gold
229 standard CFA. Extrapolating histopathological data to all 30 the mice in our experiment, we
230 would expect however that the synthetic adjuvant produced less pathology in the spinal cord on

231 average since EAE scores were lower on average. Whether this quantitative difference between
232 CFA and the synthetic formulation can be reduced with rigorous dose optimization is unclear.
233

234 Discussion

235
236 The ability of an adjuvant to elicit CMI can depend on ligand-receptor interactions,
237 specifically MAMP-PRR interactions. It is well appreciated since the hypothesis of Charles
238 Janeway Jr. that the host decision to mount an adaptive immune response requires genetically
239 inborn sensors to detect the presence of microbial products, or microbes by association, and that
240 this is the foundation of classical adjuvants including CFA²⁶. These interactions can be thought
241 of as an “arms race” between host and microbe, originating through antagonistic evolution in the
242 case of immune evasion²⁷. Additionally, we can imagine the case where a microbe might evolve
243 to increase a specific PRR interaction that favours a specific active immunological environment
244 necessary for its lifecycle. When mycobacteria interact with their host, either in the form of *M.*
245 *tuberculosis* infection, BCG vaccination or immunization using CFA, CMI normally occurs.
246 The immune response to mycobacteria has been attributed to its unique cell wall, especially the
247 MDP motif of PGN^{6, 7, 11, 24} and TDM^{17, 19}. We have shown in the context of CFA-induced
248 immunization and autoimmunity that synthetically produced *N*-glycolyl MDP and TDM
249 (GlcC14C18) can contribute synergistically to recapitulate the mycobacterial adjuvant effect.
250

251 There are also other mycobacterial MAMPs previously identified (and likely more yet
252 unidentified), plus a greater number of PRRs linked to these microbial products. The extent to
253 which some these MAMPs contribute to mycobacterial adjuvancy may be the subject of our
254 future studies. However, most are not yet producible synthetically. Purified ManLAM was
255 recently shown to elicit EAE in mice, dependent on the host C-type lectin Dectin-2 (Clec4n), at a
256 dose of 500 µg per animal²⁸. Of note, we were not able yet to produce synthetic mimics of
257 ManLAM that induce Dectin-2 signaling²⁹. Similarly, purified TDM has been used to elicit
258 EAE at 500 µg per mouse, mostly dependent on MCL (Clec4d) and partially on Mincle (Clec4e)
259¹⁹. These findings support a role for mycobacterial MAMPs driving the CFA effect, but with the
260 requirement of purifying biologically-sourced MAMPs and such high doses, we are concerned
261 that these phenotypes might be partly driven by the inclusion of other contaminating MAMPs,
262 which we have shown can have activity between 1-10 µg *in vivo* when used synergistically (i.e.
263 even 1% impurity could alter results). TLR-2 has been documented to interact with multiple
264 mycobacterial lipids³⁰. TLR-2 knockout mice have been used in EAE, but the literature is
265 inconsistent on whether TLR-2 promotes CFA-induced EAE^{31, 32, 33, 34}. Mycobacterial DNA was
266 recently shown to signal through the cGAS/STING pathway after phagosomal disruption via
267 ESX-1^{35, 36}. In the context of Freund’s adjuvant, it is not clear if heat-killed mycobacteria could
268 have cytosolic access to activate cGAS/STING. The IFA fraction perhaps could deliver MAMPs
269 across membranes. TLR-9 also senses DNA, and appears to play a role during *M. tuberculosis*
270 infection in mice³⁷, and in humans³⁸. TLR-9 was also shown to be necessary for full induction
271 of EAE^{31, 33}. As synthetic DNA is available, pursuing the role of DNA in mycobacterial
272 adjuvancy interests us, perhaps as a third synthetic MAMP to work with MDP and GlcC14C18.
273

274 Mycobacteria are not completely unique in possessing MAMPs that elicit CMI. As an
275 example, the tuberculosis vaccine candidate M72/AS01E utilizes monophosphoryl lipid A
276 (MPLA), a TLR-4 agonist based on lipopolysaccharide (LPS), to elicit CMI. LPS is made in

277 Gram negative bacteria, not mycobacteria. We concede that many microbes likely contain
278 MAMPs able to elicit CMI; here we have concerned ourselves primarily with the history of
279 mycobacterial adjuvancy and Jules Freund. It is conceivable that a combination of MAMPs
280 from different bacteria could elicit ‘unnatural’ immunity that may be beneficial to control certain
281 infectious agents that otherwise evade natural immune responses.

282
283 We were able to show that *N*-glycolylation of *M. tuberculosis* PGN altered the adjuvancy
284 of the mycobacterial cell in the context of CFA. This is consistent with our previous work on the
285 increased potency of mycobacterial PGN in other contexts^{7, 11}. Interestingly, the benefit of *N*-
286 glycolylation of PGN seemed primarily skewed toward IFN- γ production, and other Th
287 cytokines showed limited change. This may indicate that mycobacteria retain *N*-glycolylation of
288 PGN specifically to shift immune responses in a Th1 bias and should be further investigated
289 during live infection. Corroboratively, *Nod2* was also necessary for full CFA adjuvancy, for
290 IFN- γ but also cytokines indicative of other Th cell functionality. Together, this supports a role
291 of mycobacterial PGN uniquely contributing to CFA adjuvancy. We were somewhat surprised
292 that MDP emulsified by itself in IFA was insufficient to recapitulate the adjuvant effect of CFA.
293 In a 1975 paper, *N*-acetyl MDP appeared sufficient in a guinea pig model to elicit DTH using
294 OVA as antigen⁶. In 2009 using a very similar model, *N*-glycolyl MDP alone was sufficient to
295 increase ELISpot IFN- γ to near CFA levels, while *N*-acetyl MDP failed⁷. One hypothesized
296 explanation is the presence of contaminating MAMPs in certain preparations of OVA. To limit
297 this potential issue, in the current investigations we have used Endotoxin-free/ultra-pure OVA.
298 OVA is known to often come with a dose of endotoxin which affects the immunological
299 outcome of experiments³⁹. MDP alone was clearly not sufficient for us in our recent studies,
300 and this is consistent with a large literature of *in vitro* experiments that show MDP works
301 synergistically in most cellular responses.

302
303 Other groups have supported a role for TDM in mycobacterial adjuvancy^{17, 19}. TDM
304 together with purified PGN was shown to synergistically promote IL-17 production from OVA-
305 specific (OT-II) CD4+ T cells adoptively transferred into congenic mice¹⁷. This and other work
306 directed us to test Mincle-dependence of CFA and MDP synergy with TDM. *Mincle*^{-/-} mice
307 allowed us to infer that CFA adjuvancy required TDM for maximal effect for different Th-
308 indicative cytokines including IFN- γ and IL-17A. TDM is thought to be the main Mincle ligand
309 in mycobacteria, however, there are other ligands. Purified from H37Rv, trehalose-6,6'-
310 monomycolate, glucose monomycolate, diacyl-trehalose and triacyl-trehalose were shown to
311 stimulate mouse and human Mincle (plus glycerol monomycolate stimulates human Mincle only)
312²³. It is possible that the phenotype of reduced immunity is because sensing of these other
313 MAMPs is decreased. Nevertheless, we have shown Mincle signalling is essential for full CFA
314 adjuvancy.

315
316 While *in vitro* assays showed clear synergy between TDM and MDP, *in vivo* experiments
317 were limited by overt immunopathology from TDM. That TDM was able to synergize with
318 MDP drove us to test GlcC14C18, which had been branded as a similarly efficacious, but non-
319 toxic Mincle agonist²³. GlcC14C18 together with *N*-glycolyl MDP was able to partly
320 recapitulate CFA in the OVA model. Note also that the individual MAMPs had limited effect,
321 and only together substantially showed complementation of IFA. This ‘synergy’ has excited us,
322 and we are interested in further understanding the implications for MAMP signalling (which

323 MAMPs synergize together; what redundancy exists; do different synergies alter the Th type of
324 CMI? Etc.). It is unclear why MDP plus GlcC14C18 completely complemented IL-4 and IL-10,
325 while CFA immunized *Nod2*^{-/-} and *Mincle*^{-/-} mice showed only small, generally insignificant
326 defects for IL-4 and IL-10 compared to wild-type. Natural TDM might lack promotion of IL-
327 4/IL-10 axes of Th immunity, consistent with the observed ‘toxicity’. IFN- γ and IL-17A were
328 not fully complemented with the tested doses of MDP and GlcC14C18. An optimal, or
329 mycobacterial-representative, dose of these MAMPs may not have been reached. With the
330 complexity of two MAMPs and the biological variability in our model, we did not find clearly
331 better doses than those tested in EAE. Other mycobacterial MAMPs may be necessary to fully
332 recapitulate the adjuvant effect of whole mycobacteria, which have been mentioned above.

333
334 With the wholly synthetic formulation of 10 μ g GlcC14C18 plus 30 μ g *N*-glycolyl MDP,
335 we were able to induce RR-EAE in mice that was qualitatively indistinguishable from that
336 induced with CFA (in terms of ascending paralysis induced, and spinal cord pathology), but
337 milder overall (lower average EAE scores or disease burden). That the synthetically induced
338 EAE was less severe correlated with incomplete complementation in the OVA model using the
339 synthetic adjuvant. EAE that was attempted with TDM plus MDP earlier (which worked poorly)
340 was also less potent in the OVA model than the synthetic formulation, further indicating
341 correlation between these readouts (not shown). CFA often needs to be ‘titrated’ to account for
342 batch-dependent efficacy in our experience, and EAE of the level seen with the synthetic
343 adjuvant occurs sometimes with weaker CFA batches (not shown). CFA with higher
344 concentrations of mycobacteria (i.e. 4 mg/ml) is also used when a more severe, chronic
345 progressive EAE is necessary for studies, rather than relapsing-remitting EAE⁴⁰. These facts
346 point to dosing as a means of controlling the degree of EAE, which may also be true with the
347 synthetic adjuvant. Nonetheless, the current data are sufficient to demonstrate the mycobacterial
348 component of CFA can be replaced with mycobacterial MAMPs to induce EAE. Other
349 experimental uses of CFA include the collagen-induced arthritis (CIA) model and for producing
350 specific antibodies. CIA generally takes longer and has a greater role for humoral immunity than
351 EAE which is T-cell driven, (our interest was in CMI for this study)⁴¹. Wherever mycobacterial
352 adjuvancy is useful, we suspect a synthetic adjuvant could be beneficial. Indeed, intravesical
353 injection of BCG is used to treat bladder cancer (i.e. BCG can provide MAMP-driven protection,
354 not simply antigen-specific protection). Furthermore, BCG administration to millions of babies
355 each year can protect not just against childhood tuberculosis, but non-specifically against other
356 diseases⁴².

357
358 Our work demonstrates that mycobacterial NOD2 and Mincle ligands contribute to the
359 adjuvant effect of the mycobacterial cell, and that a necessarily synergistic combination of
360 synthetic MAMPs, *N*-glycolyl MDP and GlcC14C18 can at least partly recapitulate the adjuvant
361 effect of the whole mycobacterial cell. In addition to demonstrating the first entirely synthetic
362 multi-MAMP mycobacterial adjuvant, we have outlined an approach to investigate the
363 contribution of other MAMPs to adjuvant design. Moreover, the synthetic approach may be
364 useful to probe mycobacterial immunity and immunopathogenesis.

365
366
367
368

369 **Methods**

370

371 Mice

372 C57BL/6 ('wild-type') as well as *Nod2*^{-/-} mice were obtained from Jackson laboratories and
373 were bred or used immediately for experiments. *Mincle*^{-/-} mice breeders were provided courtesy
374 of the laboratory of Christine Wells²⁵. Mice were genotyped to confirm absence of the *Dock2*
375 mutation recently reported in *Nod2*^{-/-} mice⁴³. All experiments used mice from 6 to 20 weeks of
376 age. All protocols involving mice followed the guidelines of the Canadian Council on Animal
377 Care (CCAC) and were approved by the ethics committees of the RI-MUHC.

378

379 Preparation of adjuvants and ovalbumin immunization

380 Complete and incomplete Freund's adjuvant were purchased from Sigma or Invivogen. In some
381 cases, IFA was made by the experimenter from purified mineral oil and mannide monooleate
382 (Sigma). Adjuvants were prepared on the day of immunization by emulsifying CFA (1 mg/ml
383 *M. tuberculosis*) or IFA with a PBS solution containing 1 mg/ml ovalbumin (Endofit brand,
384 invivogen) in a 1:1 ratio. Emulsification was accomplished using all-plastic syringes and
385 repeated passage through an 18-G blunt-end needle. Where IFA was complemented with
386 mycobacterial components: MDP (Invivogen) was diluted in the PBS fraction of the adjuvant
387 before emulsification; TDM (Sigma) or GlcC14C18²³ were dissolved in the IFA fraction before
388 emulsification as described previously¹⁷; heat-killed mycobacteria in saline were diluted in PBS
389 and added to the PBS fraction of the adjuvant before emulsification for mice to receive an
390 equivalent of 10⁸ CFU. To make heat-killed mycobacteria, cultures were grown to equivalent
391 600-nm absorbance at mid-log phase, were pelleted and washed three times with saline, then
392 heat-killed at 100°C for 30 minutes and frozen at -80°C until use. Mice were injected
393 subcutaneously with 100 µl adjuvant-antigen emulsions in the tail 1-2 cm from the body, towards
394 the body, for sufficient and consistent drainage to the inguinal lymph nodes. Seven days after
395 injection mice were euthanized and organs were harvested for analysis.

396

397 ELISpot and flow cytometry of lymph node cells

398 Lymph nodes extracted from immunized mice were gently crushed over 70-µm cell strainers to
399 release the cells therein. Cell concentrations were determined by counting with a
400 haemocytometer or with a BD Accuri flow cytometer. Lymph node cells (LNCs) were washed
401 in culture medium, counted and cultured in 100 µl RPMI + 10%FBS (R10) at 250,000 or
402 500,000 cells per well in IFNγ ELISpot plates (R&D Systems) with or without 100 µg OVA for
403 ~40 hours at 37°C 5% CO₂ before developing the ELISpot plates. For flow cytometry analysis,
404 washed LNCs were cultured at 6 million cells per ml in 200 µl R10 with or without 200 µg OVA
405 for ~40 hours at 37°C 5% CO₂, Brefeldin A (GolgiPlugTM, BD) was added for an additional 5
406 hours, and then cells were stained and fixed (BD fixation/permeabilization buffer) for flow
407 cytometry on ice. Intracellular staining was performed on the same or the next day using BD
408 permeabilization buffer. See Table 1 for antibodies used for flow cytometry. A BD Fortessa
409 X20 was used for cellular phenotyping.

410

411 Relapsing-remitting experimental autoimmune encephalomyelitis (RR-EAE)

412 Adjuvants were prepared similarly as above, but with myelin oligodendrocyte glycoprotein
413 (MOG) used as antigen. Briefly, PBS solution containing 1 mg/ml MOG +/- 600 µg/ml *N*-
414 glycolyl MDP was emulsified with CFA (1 mg/ml *M. tuberculosis*) / IFA plus 200 µg/ml

415 GlcC14C18 (or 20 $\mu\text{g/ml}$ TDM) by back-and-forth extrusion through an 18 G two-way needle
416 with two all-plastic syringes. 8-12 week old female C57BL/6 mice (Charles River) were induced
417 for RR-EAE by a standard protocol: briefly, on day 0, pertussis toxin (PT) (200 ng) was
418 administered i.v. in the tail vein, and mice were immunized with 50 μg MOG by bilateral s.c.
419 injection in the back towards the tail with 100 μl total of an emulsification of CFA or IFA plus
420 mycobacterial MAMPs. On day 2, mice received a second equivalent dose of PT i.v.. After
421 about one week, EAE was scored blinded (i.e. the scorer did not know the adjuvant received by
422 the mouse) every day according to these cumulative criteria: 0, no paralysis (normal); 0.5, partial
423 tail weakness observed as < 50% of tail dragging when mouse walks; 1, tail paralysis observed
424 as >50% of tail dragging as mouse walks; 2, slow righting reflex (delay < 5 seconds) when
425 mouse is flipped; 3, very slow or absent righting reflex (> 5 seconds) or inability to bear weight
426 with back legs observed as dragging hindquarters when walking; 3.5, partial paralysis of one or
427 both hind limbs; 4, complete paralysis of one or both hindlimbs; 4.5, complete paralysis of one
428 or both hind limbs plus trunk weakness; 5, weakness or paralysis of forelimbs; 6, found dead.
429 Mice were weighed every other day during scoring. Mice reaching a score of 5 were euthanized
430 within 24 hours. Blinding was accomplished by having one person inject the mice and another
431 person score/weigh the mice, unaware of experimental group.

432

433 Histopathology

434 At the end of EAE scoring, the experiment was un-blinded and three mice from each group with
435 matching scores were selected. These six mice were anesthetized with peritoneal ketamine
436 injection, were perfused with PBS and formalin, and then spinal cords were extracted,
437 equilibrated in sucrose and then frozen in OTC compound (VWR). Frozen tissue was sectioned
438 14-nm thick onto slides and then stained (Nissl or Luxol fast blue). Sections of good quality (20
439 per mouse, 5 cervical, 5 upper thoracic, 5 lower thoracic and 5 lumbar) were randomly selected
440 and photographed with a Nikon Eclipse microscope. Randomized (blinded) Nissl stain
441 photographs were used to quantify the area of disease in the spinal cord by subtracting the total
442 2D area of each tissue section with the area without cellular infiltration in white matter (thus, the
443 difference of areas is the area with cellular infiltration). This was divided by the total area to
444 determine the fraction or percent of diseased area.

445

446 Software, data analysis and statistics

447 Flow cytometry data was acquired using FACSDivaTM software (BD). FCS files were analyzed
448 using FlowJo V10 (BD). Digital microscopy images were analyzed with ImageJ (NIH). Graphs
449 were generated with, and routine statistical testing was accomplished with GraphPad Prism v7 or
450 v8 (GraphPad Software Inc.). Assessment for normal data, then parametric or non-parametric
451 analyses were applied, as indicated. Sample-size and power calculations were performed
452 manually using Microsoft Excel. Manuscript figures were assembled with Microsoft
453 PowerPoint.

454

455 **References**

456

- 457 1. Chase MW, Landsteiner K. Experiments on Transfer of Cutaneous Sensitivity to Simple
458 Compounds. *Proc Soc Exp Biol Med* **49**, 688-690 (1942).

459

- 460 2. Chase MW. The Cellular Transfer of Cutaneous Hypersensitivity to Tuberculin. *Proc Soc*
461 *Exp Biol Med* **59**, 134-135 (1945).
- 462
- 463 3. Baxter AG. The origin and application of experimental autoimmune encephalomyelitis.
464 *Nat Rev Immunol* **7**, 904-912 (2007).
- 465
- 466 4. Constantinescu CS, Farooqi N, O'Brien K, Gran B. Experimental autoimmune
467 encephalomyelitis (EAE) as a model for multiple sclerosis (MS). *Br J Pharmacol* **164**,
468 1079-1106 (2011).
- 469
- 470 5. Vogel FR. Improving Vaccine Performance with Adjuvants. *Clin Infect Dis* **30**, S266–
471 270 (2000).
- 472
- 473 6. Adam A, Ellouz F, Ciorbaru R, Petit JF, Lederer E. Peptidoglycan adjuvants: minimal
474 structure required for activity. *Z Immunitätsforsch Exp Klin Immunol* **149**, 341-348
475 (1975).
- 476
- 477 7. Coulombe F, *et al.* Increased NOD2-mediated recognition of *N*-glycolyl muramyl
478 dipeptide. *J Exp Med* **206**, 1709-1716 (2009).
- 479
- 480 8. Raymond JB, Mahapatra S, Crick DC, Pavelka MS, Jr. Identification of the *namH* gene,
481 encoding the hydroxylase responsible for the *N*-glycolylation of the mycobacterial
482 peptidoglycan. *J Biol Chem* **280**, 326-333 (2005).
- 483
- 484 9. Mahapatra S, Crick DC, McNeil MR, Brennan PJ. Unique structural features of the
485 peptidoglycan of *Mycobacterium leprae*. *J Bacteriol* **190**, 655-661 (2008).
- 486
- 487 10. Essers L, Schoop HJ. Evidence for the incorporation of molecular oxygen, a pathway in
488 biosynthesis of *N*-glycolylmuramic acid in *Mycobacterium phlei*. *Biochim Biophys Acta*
489 **544**, 180-184 (1978).
- 490
- 491 11. Hansen JM, *et al.* *N*-glycolylated peptidoglycan contributes to the immunogenicity but
492 not pathogenicity of *Mycobacterium tuberculosis*. *J Infect Dis* **209**, 1045-1054 (2014).
- 493
- 494 12. Girardin SE, *et al.* *Nod2* is a general sensor of peptidoglycan through muramyl dipeptide
495 (MDP) detection. *J Biol Chem* **278**, 8869-8872 (2003).
- 496
- 497 13. Miceli-Richard C, *et al.* CARD15 mutations in Blau syndrome. *Nat Genet* **29**, 19-20
498 (2001).
- 499

- 500 14. Ogura Y, *et al.* A frameshift mutation in NOD2 associated with susceptibility to Crohn's
501 disease. *Nat Lett* **411**, 603-606 (2001).
- 502
- 503 15. Austin CM, Ma X, Graviss EA. Common nonsynonymous polymorphisms in the NOD2
504 gene are associated with resistance or susceptibility to tuberculosis disease in African
505 Americans. *J Infect Dis* **197**, 1713-1716 (2008).
- 506
- 507 16. Zhang FR, *et al.* Genomewide association study of leprosy. *N Engl J Med* **361**, 2609-
508 2618 (2009).
- 509
- 510 17. Shenderov K, *et al.* Cord factor and peptidoglycan recapitulate the Th17-promoting
511 adjuvant activity of mycobacteria through Mincle/CARD9 signaling and the
512 inflammasome. *J Immunol* **190**, 5722-5730 (2013).
- 513
- 514 18. Ishikawa E, *et al.* Direct recognition of the mycobacterial glycolipid, trehalose
515 dimycolate, by C-type lectin Mincle. *J Exp Med* **206**, 2879-2888 (2009).
- 516
- 517 19. Miyake Y, *et al.* C-type lectin MCL is an FcRgamma-coupled receptor that mediates the
518 adjuvanticity of mycobacterial cord factor. *Immunity* **38**, 1050-1062 (2013).
- 519
- 520 20. Bekierkunst A. Acute Granulomatous Response Produced in Mice by Trehalose-6,6-
521 Dimycolate. *J Bacteriol* **96**, 958-961 (1968).
- 522
- 523 21. Shigeru K, Tsunehiko F, Hidefumi Y, Masahiko F, Ichiro A, Yuichi Y. Synthesis of
524 Muramyl Dipeptide Analogs with Enhanced Adjuvant Activity. *Bull Chem Soc Japan* **53**,
525 2570-2577 (1980).
- 526
- 527 22. Xing S, Gleason JL. A robust synthesis of N-glycolyl muramyl dipeptide via
528 azidonitration/reduction. *Org Biomol Chem* **13**, 1515-1520 (2015).
- 529
- 530 23. Decout A, *et al.* Rational design of adjuvants targeting the C-type lectin Mincle. *Proc*
531 *Natl Acad Sci U S A* **114**, 2675-2680 (2017).
- 532
- 533 24. Divangahi M, *et al.* NOD2-Deficient Mice Have Impaired Resistance to Mycobacterium
534 tuberculosis Infection through Defective Innate and Adaptive Immunity. *J Immunol* **181**,
535 7157-7165 (2008).
- 536
- 537 25. Wells CA, *et al.* The Macrophage-Inducible C-Type Lectin, Mincle, Is an Essential
538 Component of the Innate Immune Response to *Candida albicans*. *The Journal of*
539 *Immunology* **180**, 7404-7413 (2008).

- 540
541 26. Janeway CA. Approaching the Asymptote? Evolution and Revolution in Immunology.
542 *Cold Spring Harb Symp Quant Biol* **54**, 1-13 (1989).
- 543
544 27. Odendall C, Kagan JC. Host-Encoded Sensors of Bacteria: Our Windows into the
545 Microbial World. *MicrobiolSpectrum* **7**, (2019).
- 546
547 28. Yonekawa A, *et al.* Dectin-2 Is a Direct Receptor for Mannose-Capped
548 Lipoarabinomannan of Mycobacteria. *Immunity* **41**, 402–413 (2014).
- 549
550 29. Decout A, *et al.* Deciphering the molecular basis of mycobacteria and lipoglycan
551 recognition by the C-type lectin Dectin-2. *Sci Rep* **8**, 16840 (2018).
- 552
553 30. Stamm CE, Collins AC, Shiloh MU. Sensing of Mycobacterium tuberculosis and
554 consequences to both host and bacillus. *Immunol Rev* **264**, 204-219 (2015).
- 555
556 31. Prinz M, *et al.* Innate immunity mediated by TLR9 modulates pathogenicity in an animal
557 model of multiple sclerosis. *J Clin Invest* **116**, 456-464 (2006).
- 558
559 32. Reynolds JM, *et al.* Toll-like receptor 2 signaling in CD4(+) T lymphocytes promotes T
560 helper 17 responses and regulates the pathogenesis of autoimmune disease. *Immunity* **32**,
561 692-702 (2010).
- 562
563 33. Miranda-Hernandez S, *et al.* Role for MyD88, TLR2 and TLR9 but not TLR1, TLR4 or
564 TLR6 in experimental autoimmune encephalomyelitis. *J Immunol* **187**, 791-804 (2011).
- 565
566 34. Shaw PJ, *et al.* Signaling via the RIP2 adaptor protein in central nervous system-
567 infiltrating dendritic cells promotes inflammation and autoimmunity. *Immunity* **34**, 75-84
568 (2011).
- 569
570 35. Collins Angela C, *et al.* Cyclic GMP-AMP Synthase Is an Innate Immune DNA Sensor
571 for Mycobacterium tuberculosis. *Cell Host & Microbe* **17**, 820-828 (2015).
- 572
573 36. Watson Robert O, *et al.* The Cytosolic Sensor cGAS Detects Mycobacterium tuberculosis
574 DNA to Induce Type I Interferons and Activate Autophagy. *Cell Host & Microbe* **17**,
575 811-819 (2015).
- 576
577 37. Bafica A, Scanga CA, Feng CG, Leifer C, Cheever A, Sher A. TLR9 regulates Th1
578 responses and cooperates with TLR2 in mediating optimal resistance to Mycobacterium
579 tuberculosis. *J Exp Med* **202**, 1715-1724 (2005).

- 580
581 38. Chen Z, Wang W, Liang J, Wang J, Feng S, Zhang G. Association between toll-like
582 receptors 9 (TLR9) gene polymorphism and risk of pulmonary tuberculosis: meta-
583 analysis. *BMC Pulm Med* **15**, 57 (2015).
- 584
585 39. Eisenbarth SC, Piggott DA, Huleatt JW, Visintin I, Herrick CA, Bottomly K.
586 Lipopolysaccharide-enhanced, toll-like receptor 4-dependent T helper cell type 2
587 responses to inhaled antigen. *J Exp Med* **196**, 1645-1651 (2002).
- 588
589 40. Berard JL, Wolak K, Fournier S, David S. Characterization of relapsing-remitting and
590 chronic forms of experimental autoimmune encephalomyelitis in C57BL/6 mice. *Glia* **58**,
591 434-445 (2010).
- 592
593 41. Brand DD, Latham KA, Rosloniec EF. Collagen-induced arthritis. *Nat Protoc* **2**, 1269-
594 1275 (2007).
- 595
596 42. Kleinnijenhuis J, *et al.* Bacille Calmette-Guerin induces NOD2-dependent nonspecific
597 protection from reinfection via epigenetic reprogramming of monocytes. *Proc Natl Acad*
598 *Sci U S A* **109**, 17537-17542 (2012).
- 599
600 43. Wong SY, *et al.* B Cell Defects Observed in Nod2 Knockout Mice Are a Consequence of
601 a Dock2 Mutation Frequently Found in Inbred Strains. *J Immunol* **201**, 1442-1451
602 (2018).

603

604 **Acknowledgments**

605

606 We would like to thank the Containment Level 3 platform of the Research Institute of the
607 McGill University Health Centre (RI-MUHC) for providing the needed facilities and intellectual
608 support. Similarly, we thank the Immunophenotyping platform of the RI-MUHC for cytometers
609 and advice. We are very grateful to Christine Wells (University of Melbourne, Australia) for
610 providing *Mincle*-KO mice and to Alexiane Decout for preparing GlcC14C18. For tutelage and
611 technical assistance, J.Y.D. is thankful to Damien Montamat-Sicotte, Ourania Tsatas, Sarah
612 Danchuk, Iain Roe, Andréanne Lupien, Nimara Asbah, and Daniel Houle. J.Y.D. was personally
613 supported by the Canadian Institutes of Health Research (CIHR) Canada Graduate Scholarship –
614 Master’s Program, Fonds de Recherche du Québec – Santé (FRQ-S) Doctoral Training Award,
615 RI-MUHC studentships (Master’s and Ph.D.) and scholarships from the McGill Department of
616 Microbiology and Immunology. Research activities were funded by CIHR foundation grant held
617 by M.B. and a CIHR grant held by S.D.

618

619 **Author Contributions**

620

621 Conceptualization, J.Y.D. and M.B.; Methodology, J.Y.D. and J.G.Z.; Investigation, J.Y.D.,
622 F.M. and J.G.Z.; Resources, S.D., J.N. and M.B.; Writing – Original Draft, J.Y.D. and M.B.;
623 Writing – Review & Editing, J.Y.D., F.M., J.G.Z., S.D., J.N. and M.B.; Visualization, J.Y.D.;
624 Supervision, S.D. and M.B.; Funding acquisition, J.Y.D., S.D. and M.B.

625

626 **Competing Interests**

627

628 The authors have no competing interests

629

630 **Figure Legends**

631

632 **Figure 1. CFA-dependent cell-mediated immune responses as a function of mycobacterial**
633 ***namH*.** **A**, PGN of ‘wild-type’ H37Rv *M. tuberculosis* (left) and PGN of the $\Delta namH$ mutant
634 (right). The MDP motif is drawn in red, and the site of *N*-glycolylation is in bold font. With
635 NamH, *N*-glycolylation was shown on ~70% of muramic acid residues, with *N*-acetylation on the
636 remaining ~30%^{8,11}. **B**, immunization scheme (relevant to figs. 1-5): C57Bl/6J mice were
637 immunized with adjuvant emulsion containing OVA by s.c. injection at the base of the tail, and
638 after seven days, inguinal (draining) lymph nodes were harvested. Lymph node cells were
639 cultured *ex vivo* with or without OVA to examine OVA-specific cytokine response by flow
640 cytometry or ELISpot. **C**, cytokine production from CD4+CD8- lymph node cells of mice
641 immunized against OVA with heat-killed *M. tuberculosis* strain H37Rv, H37Rv $\Delta namH$, or IFA
642 alone, seven days prior. Shown are data pooled from four separate experiments, from individual
643 mice, with averages +/- SEM. p-values were calculated with two-tailed student’s t-tests.
644 *p<0.05; **p<0.01; ns, not significant, p>0.05. For IFA + H37Rv, IFA + H37Rv $\Delta namH$, and
645 IFA alone, N = 31, 27 and 16, respectively.

646

647 **Figure 2. CFA-dependent cell-mediated immune responses as a function of host *Nod2*.**

648 Cytokine production from CD4+CD8- lymph node cells of *Nod2*^{+/+} and *Nod2*^{-/-} mice
649 immunized against OVA with CFA or IFA seven days prior. Shown are data representative of
650 two independent experiments, from individual mice with averages +/- SEM. p-values were
651 calculated with two-tailed student’s t-tests. *p<0.05; **p<0.01; ns, not significant, p>0.05. For
652 CFA *Nod2*^{+/+}, CFA *Nod2*^{-/-}, IFA *Nod2*^{+/+} and IFA *Nod2*^{-/-}, N = 12, 13, 9 and 7, respectively.

653

654 **Figure 3. CFA-dependent cell-mediated immune responses as a function of host *Mincle*.**

655 Cytokine production from CD4+CD8- lymph node cells of *Mincle*^{+/+} and *Mincle*^{-/-} mice
656 immunized against OVA with CFA or IFA seven days prior. Shown are data pooled from two
657 independent experiments, from individual mice, with averages +/- SEM. p-values were
658 calculated with two-tailed student’s t-tests. *p<0.05; **p<0.01; ns, not significant, p>0.05. For
659 CFA *Mincle*^{+/+}, CFA *Mincle*^{-/-}, IFA *Mincle*^{+/+} and IFA *Mincle*^{-/-}, N = 14, 16, 15 and 11,
660 respectively.

661

662 **Figure 4. *Mincle*-dependent inflammation from TDM is not observed with synthetic TDM**
663 **analogue GlcC14C18.** **A**, TDM molecular structure. **B**, GlcC14C18 molecular structure. **C**,
664 representative tail injection site pathology seven days after injection of 10 μ g TDM or 10 μ g
665 GlcC14C18 in IFA-PBS emulsion. Pictures are representative of 3 mice per group.

666

667 **Figure 5. Complementation of IFA with synthetic mycobacterial MAMPs.** Cytokine
 668 production from CD4+CD8- lymph node cells of wild-type mice immunized against OVA seven
 669 days prior with IFA + 30 µg *N*-glycolyl MDP (N=6), IFA + 30 µg *N*-glycolyl MDP + 10 µg
 670 GlcC14C18 (N=7), IFA + 30 µg *N*-glycolyl MDP + 30 µg GlcC14C18 (N=7), or CFA (N=7).
 671 Shown are data from individual mice, with averages +/- SEM.

672
 673 **Figure 6. RR-EAE induced by IFA+GlcC14C18+MDP.** **A**, experimental timeline. **B**,
 674 average EAE score +/- SEM over time of mice induced with CFA (N=15) or IFA + 10 µg
 675 GlcC14C18 + 30 µg *N*-glycolyl MDP (N=15). Mice were euthanized on day 28 post injection.
 676 **C**, Cumulative EAE score, obtained by adding the EAE score of each mouse over each of the 28
 677 days. Lines represent averages +/- SEM. *p*-value was calculated with two-tailed student's *t*-
 678 tests. ***p* = 0.0022

679
 680 **Figure 7. Spinal cord pathology in RR-EAE mice induced by IFA+GlcC14C18+MDP.** **A**,
 681 Nissl and Luxol fast blue (LFB) stains of spinal cord sections from RR-EAE-induced mice at day
 682 28 post injection, having an EAE score of 3.5 upon euthanasia. Red boxes highlight cellular
 683 infiltration and spatially associated demyelination of the white matter seen by Nissl and LFB
 684 staining, respectively. **B**, Quantitative spinal cord pathology per EAE score upon euthanasia.
 685 Statistical significance was determined by Tukey's multiple comparisons test. **p*<0.05 and
 686 *****p*<0.0001 (adjusted for multiple comparisons). N=40 for each group (20 from CFA and 20
 687 from synthetic adjuvant of equivalent EAE scores). Lines indicate averages +/- SEM **C**,
 688 Quantitative spinal cord pathology per adjuvant. Statistical significance was tested with two-
 689 tailed unpaired Welch's *t*-test; a power calculation for given variances and N=60 per group
 690 indicated an ability to discern +/- 15% difference vs. CFA control. Lines indicate averages +/-
 691 SEM.

692
 693 **Tables**

694
 695 **Table 1. Flow cytometry antibodies**

Target	Brand	Clone	Fluorochrome
CD3ε	BD	145-2C11	PE
CD4	BD	GK1.5	BV786
CD8α	BD	53-6.7	BV711
CD19	Biolegend	6D5	PE-Dazzle594
B220/CD45R	BD	RA3-6B2	BUV737
IFN-γ	Biolegend	XMG1.2	APC
IL-2	BD	JES6-5H4	BV605
IL-4	eBiosciences	BVD6-24G2	PE-Cy7
IL-17A	BD	TC11-18H10	BUV395
IL-10	BD	JES5-16E3	FITC

696
 697
 698
 699
 700
 701

702 **Supplementary Information**

703

704 Supplemental Method: Bone marrow-derived dendritic cells (BMDCs)

705 Bone marrow was extracted from mice by flushing femora and tibiae with PBS + 2% BSA + 2%
706 glucose using a 25-G syringe. Red blood cells were lysed and remaining bone marrow cells
707 were filtered through 70 μ m cell strainer. Cells were cultured at 500,000 cells / ml R10 with 20
708 ng/ml murine rGM-CSF (PeproTech); cells were fed on day 3 with R10 + rGM-CSF, and on day
709 6 with R10 alone. On day 7, loosely adherent cells were harvested by gentle pipetting and used
710 in assays.

711

712 Supplemental Figure Legends

713

714 **Figure S1. Flow cytometry gating strategy for lymph node cells.** Shown is representative
715 gating and data from an OVA-stimulated sample.

716

717 **Figure S2. CFA-dependent lymphoproliferation, IL-4 and IL-10 as a function of**
718 **mycobacterial *namH*.** These data are from the same set shown in fig. 1B (refer to fig. 1B
719 legend for details). p-values were calculated with two-tailed student's t-tests.

720

721 **Figure S3. Contribution of *namH* to the mycobacterial portion of OVA-specific IFN- γ**
722 **elicited by CFA.** These transformed data are from the same set shown in fig. 1B (refer to fig.
723 1B legend for details). **A**, result was obtained from %IFN- γ + data by subtracting the average
724 IFA background from all CFA data, and plotting the results as % of IFA+H37Rv 'wild-type'. **B**,
725 result was obtained from # IFN- γ + data by subtracting the average IFA background from all
726 CFA data, and plotting the results as % of IFA+H37Rv 'wild-type'.

727

728 **Figure S4. CFA-dependent ELISpot IFN- γ , lymphoproliferation, IL-4 and IL-10 as a**
729 **function of host *Nod2*.** **A**, IFN- γ ELISpot of total lymph node cells of immunized mice
730 produced in an independent experiment. p-values were calculated with two-tailed student's t-
731 tests. *p<0.05 and ***p<0.0005. For CFA *Nod2*+/+, CFA *Nod2*-/-, IFA *Nod2*+/+ and IFA
732 *Nod2*-/-, N = 6, 8, 6 and 6, respectively. **B-C**, data are from the same set shown in fig. 2 (refer to
733 fig. 2 legend for details).

734

735 **Figure S5. CFA-dependent lymphoproliferation, IL-4 and IL-10 as a function of host**
736 ***Mincle*.** These data are from the same set shown in fig. 3 (refer to fig. 3 legend for details).

737

738 **Figure S6. TDM-induced injection site pathology.** Tail injection site pathology seven days
739 after injection of 1 μ g TDM or 10 μ g TDM in IFA-PBS emulsion, or CFA control. Pictures are
740 representative of 5 mice per group.

741

742 **Figure S7. Semi-quantification of *Mincle*-dependent inflammation from TDM.** These data
743 are from the same set shown in fig. 4C (refer to fig. 4C legend for more details). **A**, injection site
744 pathology over time (scores were given by these criteria: 0, normal; 1, any mark/discoloration at
745 site; 2, obvious swelling; 3, 2+abnormal skin). **B**, scores from A for each day added together.
746 Shown are means +/- SD. N=3 for all groups.

747

748 **Figure S8. Murine BMDCs respond to *N*-glycolyl MDP, TDM and GlcC14C18**
749 **synergistically.** 200,000 BMDCs were transferred per well into 96-well plates precoated with
750 50 ng/well of TDM or GlcC14C18 by dissolving in isopropanol and drying (lipid-free conditions
751 used wells treated with isopropanol alone). Where present, MDP is 1 μ g/ml. BMDCs were
752 incubated with stimulants for 6 hours at 37°C, 5% CO₂ before supernatant was removed for
753 ELISA analysis. Shown are averages +/- SEM of 3-6 individually stimulated and assayed wells.

754

755 **Figure S9. Adjuvant-dependent lymphoproliferation and ELISpot IFN- γ .** These data are
756 from the same set shown in fig. 5 (refer to fig. 5 legend for details).

757

758 **Figure S10. Complementation of IFA with fixed GlcC14C18 dose, increasing *N*-glycolyl**
759 **MDP dose.** **A**, lymphoproliferation and **B**, cytokine production from CD4⁺ lymph node cells of
760 wild-type mice immunized against OVA seven days prior with IFA (N=4), IFA + 10 μ g
761 GlcC14C18 (N=7), IFA + 10 μ g GlcC14C18 + 1 μ g MDP (N=6), or IFA + 10 μ g GlcC14C18 +
762 3 μ g MDP (N=7). Shown are data from individual mice, with averages +/- SEM.

763

764 **Figure S11. Descriptive statistics for RR-EAE induced by IFA+GlcC14C18+MDP.** These
765 data are from the same set shown in fig. 6 (refer to fig. 6 legend for details). **A**, average weight
766 +/- SEM over time of mice. **B**, maximum EAE score reached on any day by mice, as of day 28.
767 **C**, disease course of mice selected for spinal cord histopathology.

768

769 **Figure S12. Descriptive statistics for RR-EAE induced by IFA+TDM+MDP.** **A**, average
770 EAE score +/- SEM over time of mice induced with CFA (N=13) or IFA + 1 μ g TDM + 30 μ g
771 *N*-glycolyl MDP (N=13). Mice were euthanized on day 27 post injection. **B**, cumulative EAE
772 score, obtained by adding the EAE score of each mouse over each of the 27 days. Lines
773 represent averages +/- SEM. **C**, average weight +/- SEM over time of mice. **D**, maximum EAE
774 score reached on any day by mice, as of day 27.

FIG. 1

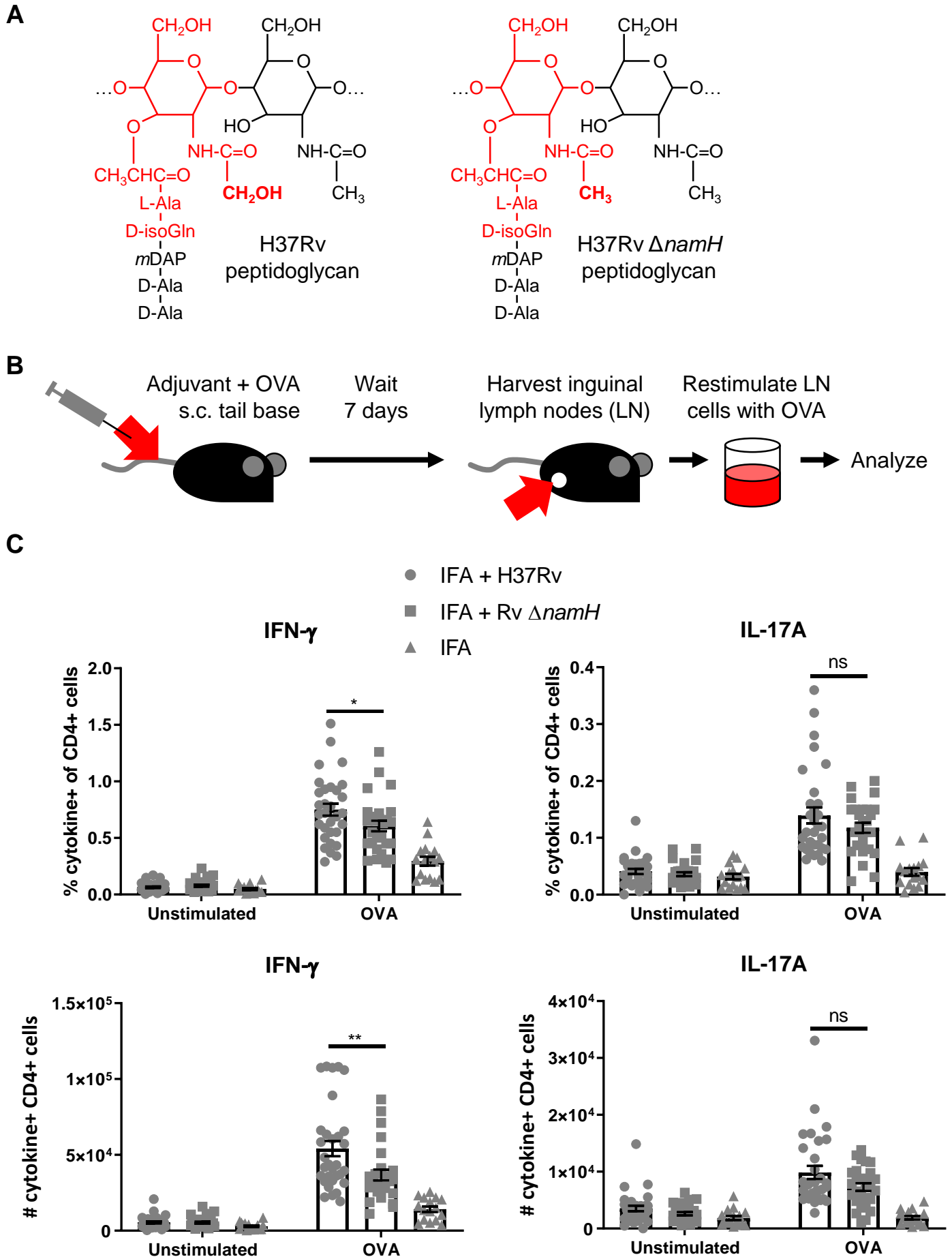


FIG. 2

- CFA *Nod2*^{+/+}
- CFA *Nod2*^{-/-}
- ▲ IFA *Nod2*^{+/+}
- ▼ IFA *Nod2*^{-/-}

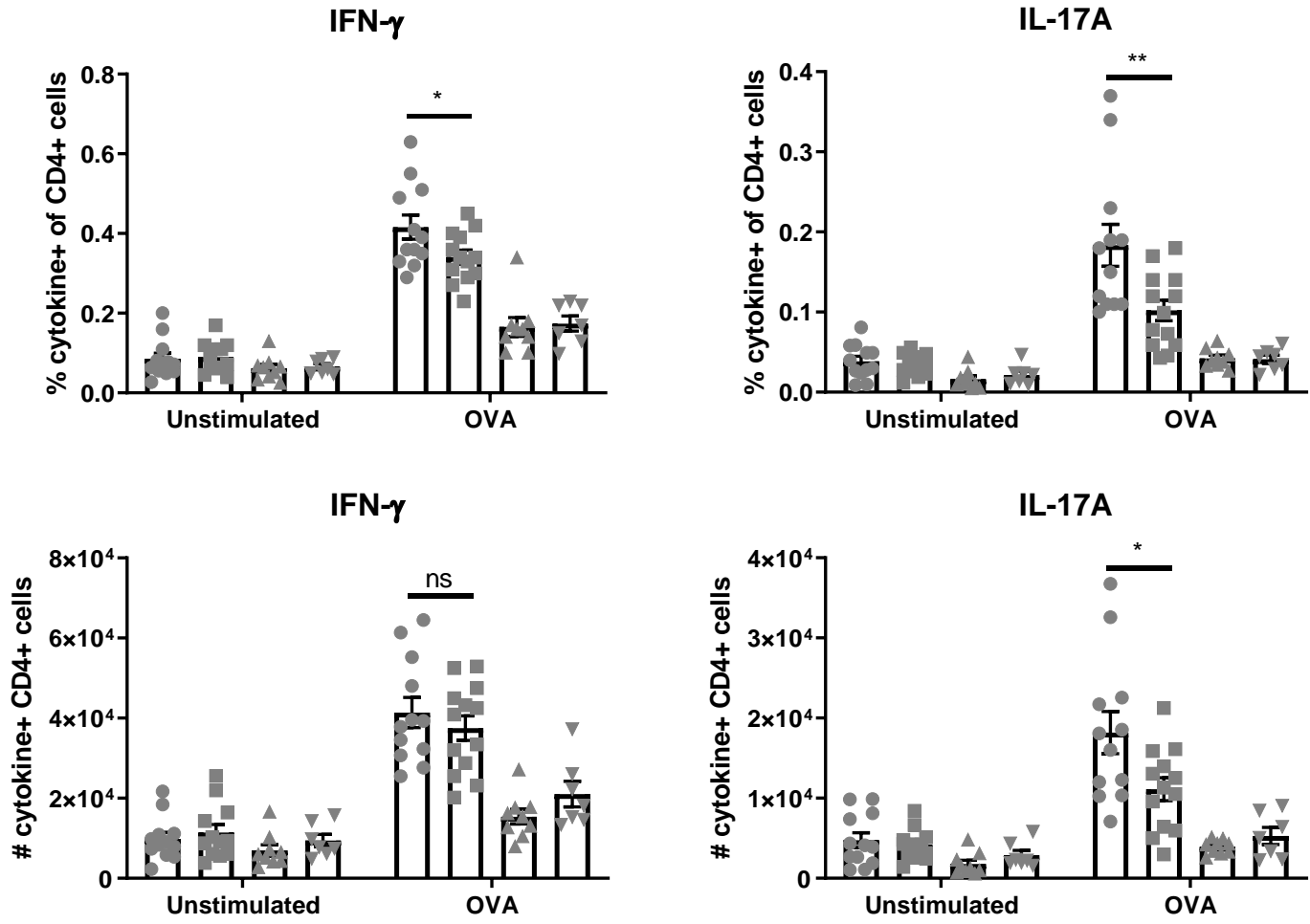


FIG. 3

- CFA *Mincle*^{+/+}
- CFA *Mincle*^{-/-}
- ▲ IFA *Mincle*^{+/+}
- ▼ IFA *Mincle*^{-/-}

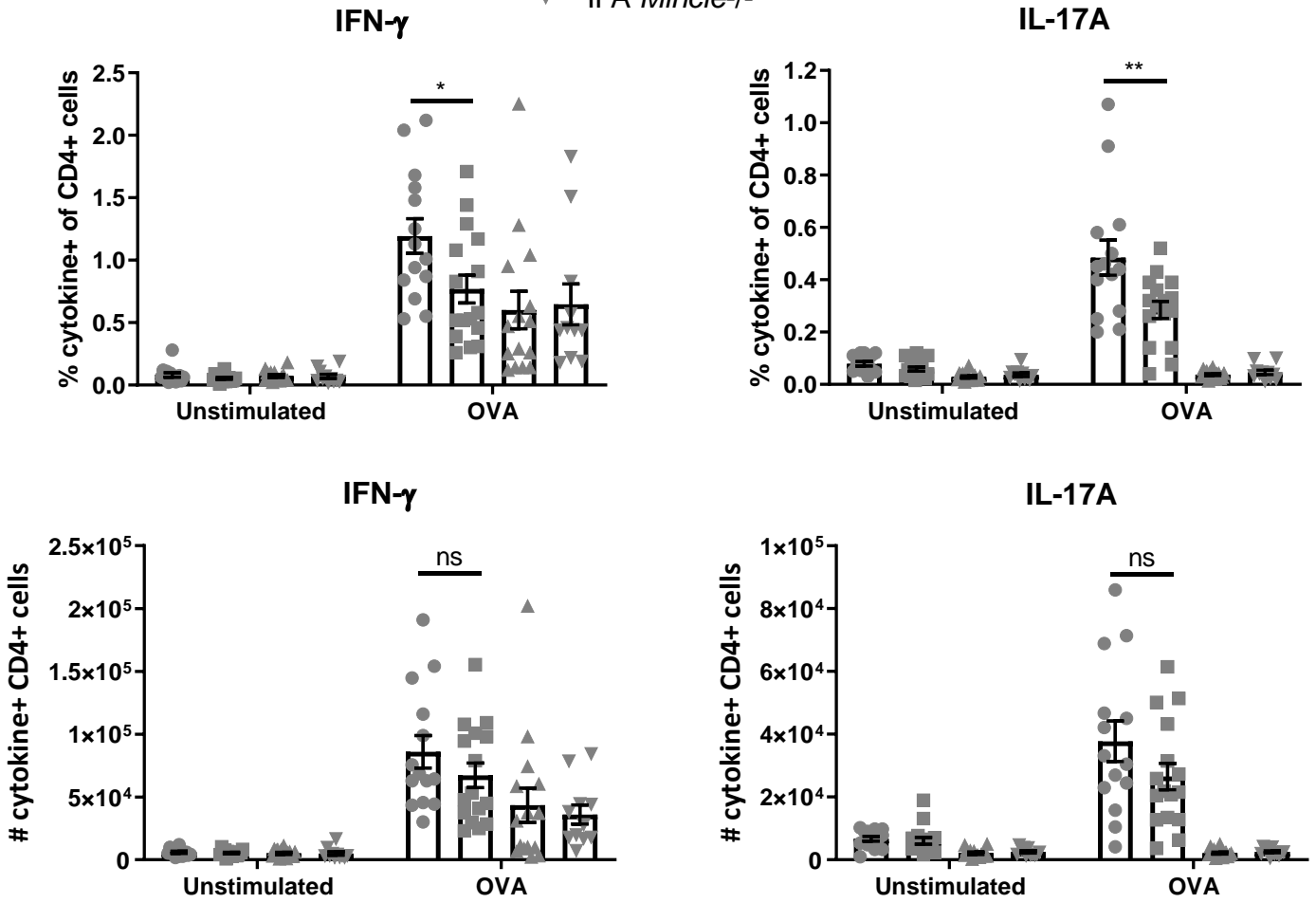
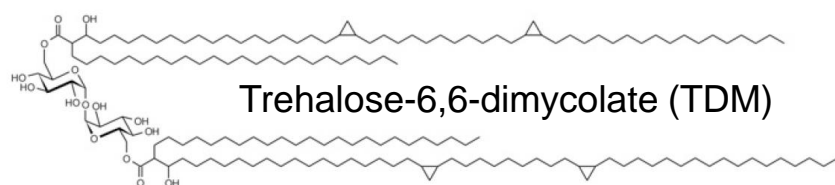
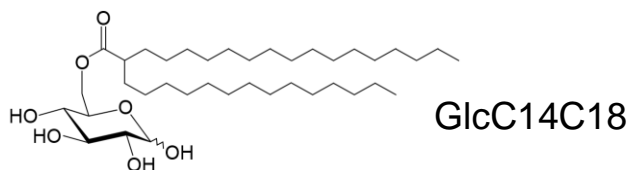


FIG. 4

A



B



C

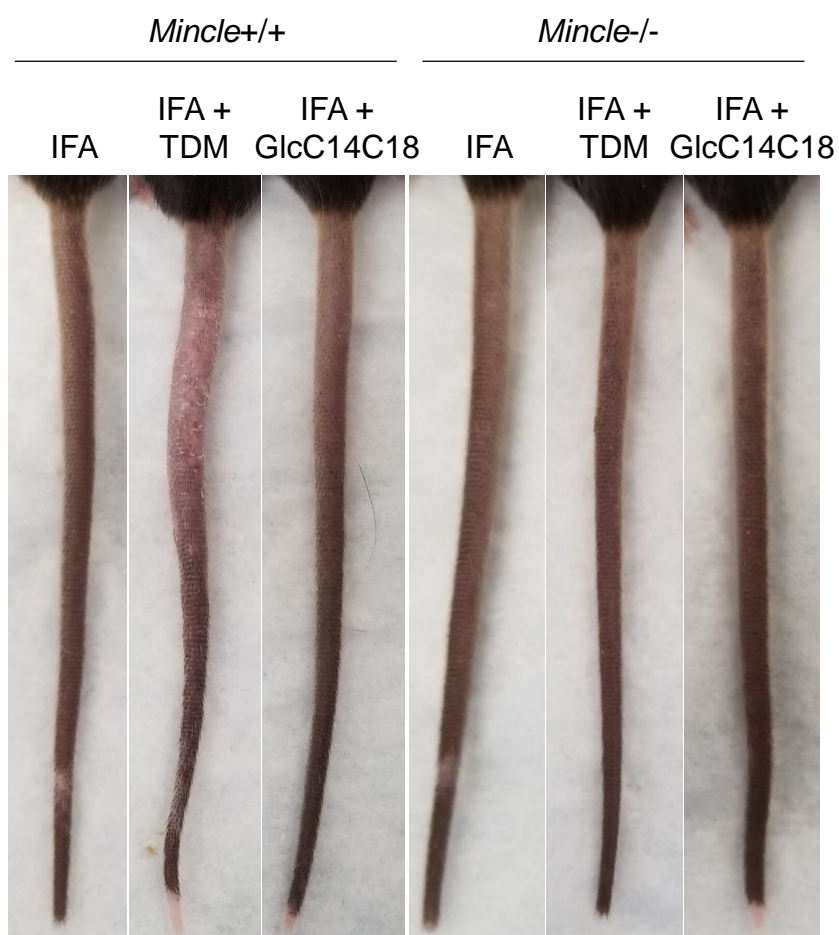


FIG. 5

- IFA + 30 μ g *N*-glycolyl MDP
- ▼ IFA + MDP + 10 μ g GlcC14C18
- ▲ IFA + MDP + 30 μ g GlcC14C18
- CFA

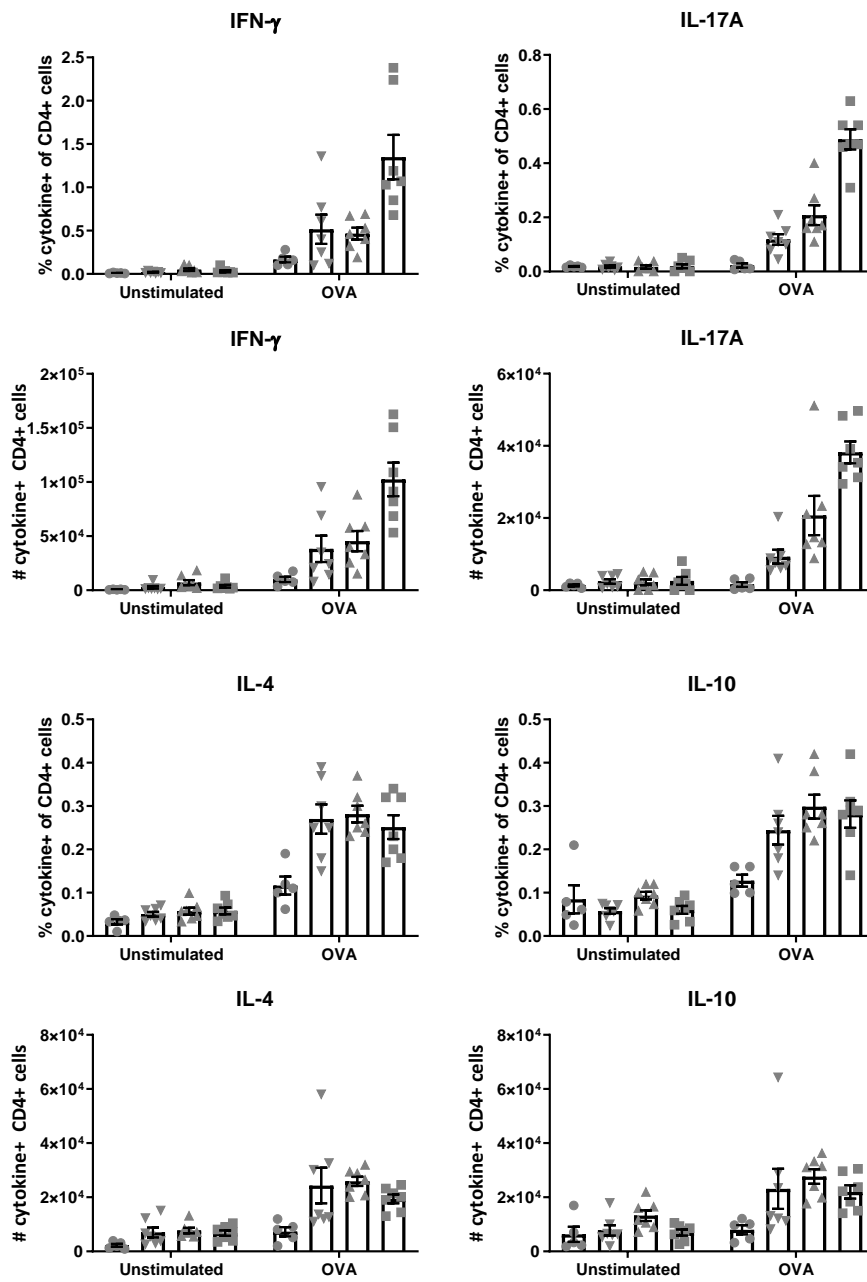


FIG. 6

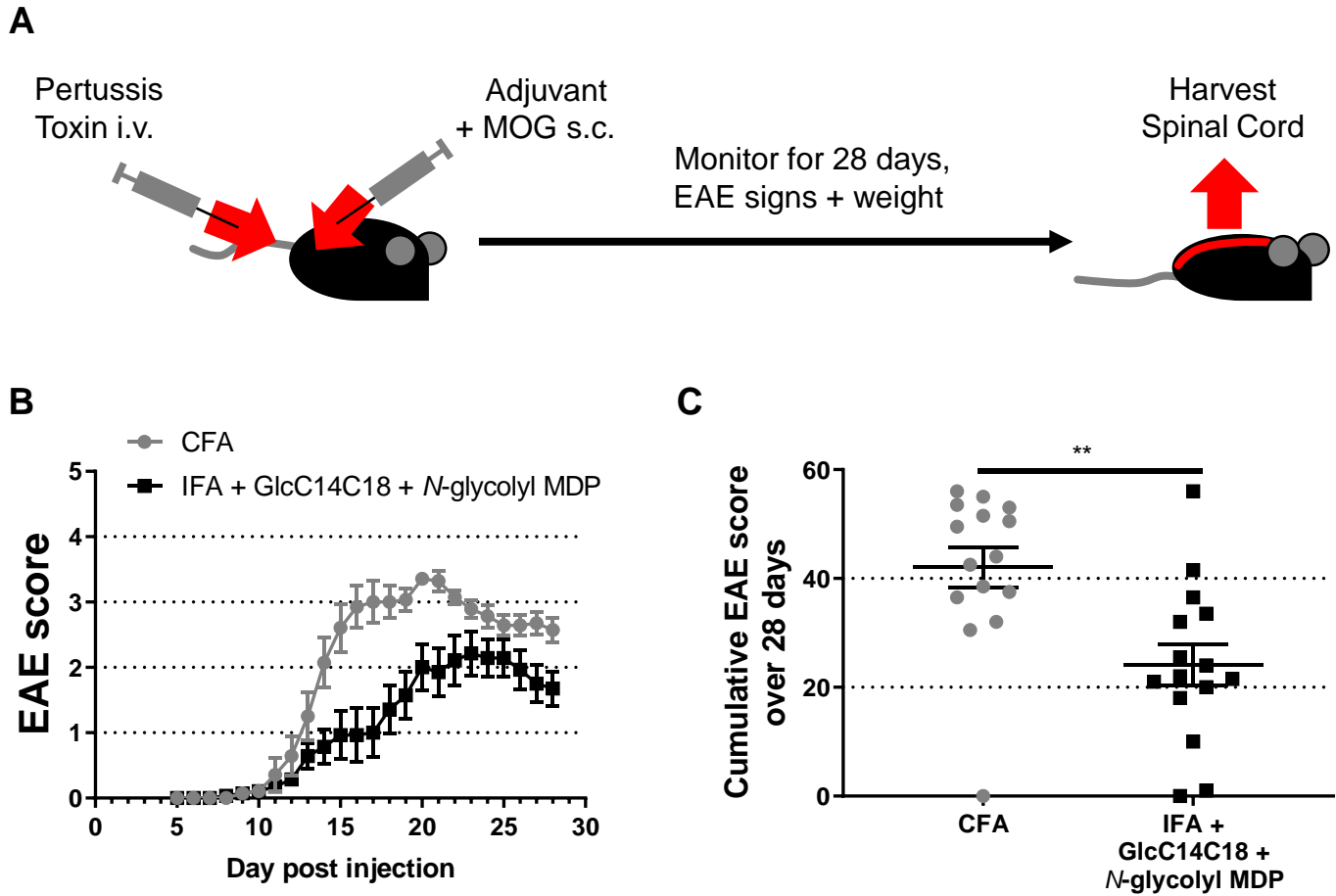


FIG. 7

